University of Auckland

Department of Engineering Science

Part IV Project

Optimal Experimental Design for Understanding Burn Injuries

FINAL RESEARCH REPORT

Author:
Marah Shahin

Supervisors:
Dr Oliver Maclaren
Dr Ruanui Nicholson
Dr Vinod Suresh

October 30, 2020

Abstract

This project computationally and mathematically investigates the optimal experimental design for measuring thermal diffusivity in the layers of skin. First, a finite element solver was constructed for the so-called forward model of a typical burn experiment. This was then embedded into a framework for parameter recovery and uncertainty quantification, that allows the estimation of skin parameters from temperature measurements. This was used to assess the quality of different designs in terms of how well they enable accurate parameter recovery. Particularly, consideration was given to: the number of measuring probes to use; the location of these probes, and the effects of including additional skin layers. This assessment uses both synthetic data as well as real data obtained from a phantom model as part of the companion parallel project. The comparison with real-world data also highlights the critical impact that model misspecification can have on the validity of parameter recovery. Many designs - with different combinations of one or two layers, and; one, two, or three probes measuring temperatures were analysed. The investigation found diffusivities past the first layer had potential identifiability issues when attempting to recover their thermal diffusivity. Hence, the optimal experimental design deduced was a one-layered phantom model that had probes at three different locations within. Multi-layered models, however, should not be discounted, the model used here should simply be revised. Ultimately, this project has laid a basis for future work to build and further improve upon.

Acknowledgments

Many thanks to Oliver for his endless, extremely useful suggestions, notes and guidance. I appreciate the time and effort you've put into my work.
I'd like to thank Ru for his enthusiasm and interest in my work. Thank you also for the help and pages of notes explaining FEM (the method would still be a mystery to me without it).
Thanks to Vinod for the feedback, advice and aid in this project.
Overall thanks to all my supervisors for the help, support and unwavering patience during this time. Thank you also for the experience from this stimulating, well-rounded project!

Special thanks to my friends and family for being my pillars during this trying, eerie year. This project wouldn't have been the same without your unparalleled support and love.

Declaration of Contribution

All work completed in this project is solely that of the student's, with the exception of the contributions listed below:

- Matplotlib, SciPy and Pandas Python packages were used.
- Python code written by Rick Fu was slightly tailored to validate a Finite Difference solver written by the student [1, 2]
- MATLAB code written by Matthew Simpson was adapted to validate a Finite Element Method written by the student [3].
- Experiments were designed, constructed and conducted by Anthony Zemke [4].

Contents

List of Figures

List of Tables

1 Introduction and Background

This project aims to investigate and understand burn injuries using both experiments and computational modelling. The present report focuses on using computational modelling to guide experimental design, while a companion report [4] focuses on developing and performing experiments using skin phantoms.

A key goal in experimental work on understanding burn injuries is recovering the main thermal parameters of the skin using real-time heat transfer experiments. Existing experiments involve several limitations and complications, such as requiring porcine (pig) skin, using a single measuring probe, and simplifying away important factors (e.g. multiple skin layers). The need to address these limitations raises protocol ambiguity. For example, it is unclear which factors are most important, where to place additional measuring probes, or what sort of designs are needed to ensure adequate estimation of the parameters of more complex multilayered tissues. Thus, this report investigates the quality of various experimental designs for burn experiments using methods from computational modelling, statistical inverse problems, and optimal experimental design.

Here the basic literature on burn injury modelling and parameter estimation is first reviewed. A more detailed literature review can be found in [5].

1.1 Burn injuries: Overview and Motivation

Burn injuries are ranked in four different degrees. A first-degree burn is considered the least severe, only affecting the skins epidermis, while a fourth-degree reaches past the skin, fat layer, muscle and bone [6]. Burns caused by heat are of the most common [7], thus are of the highest interest to investigate.
To enhance understanding of these conditions, experiments have been conducted using various methods, such as the use of heated water, infrared lasers, porcine skin or phantom models [3, 8].

1.2 Modelling Burn Injuries: The Forward Problem

Heat traveling through skin can be mathematically modelled and solved in a number of different ways. The literature review discusses a number of these models [5].
The most common is the general heat equation - originally developed by Joseph Fourier [9]. This equation was deemed the most suitable as projects with similar

models adopted the equation to produce validated results [3, 10]. The parabolic heat equation in one dimension is Equation 1:

$$\frac{\partial u}{\partial t} = \frac{\partial}{\partial x}\left(D\frac{\partial u}{\partial x}\right), \tag{1}$$

where D is the thermal diffusivity of the medium [11]. Thermal diffusivity is a parameter calculated from density, ρ, thermal conductivity, λ and the specific heat capacity, c where:

$$D = \frac{\lambda}{c\rho}. \tag{2}$$

Where relevant, the heat equation can be generalised to N spatial dimensions, as shown in Equation 3:

$$\frac{\partial u}{\partial t} = \nabla \cdot (D\nabla u). \tag{3}$$

1.3 Determining Parameters and Designing Experiments

1.3.1 Inverse Problems

A forward problem, with $F(x) = y$, finds y given x. An inverse problem on the other hand, estimates x given y. In essence, inverse problems start with effects then determine the causes. The inverse problem process can be seen in Figure 1.

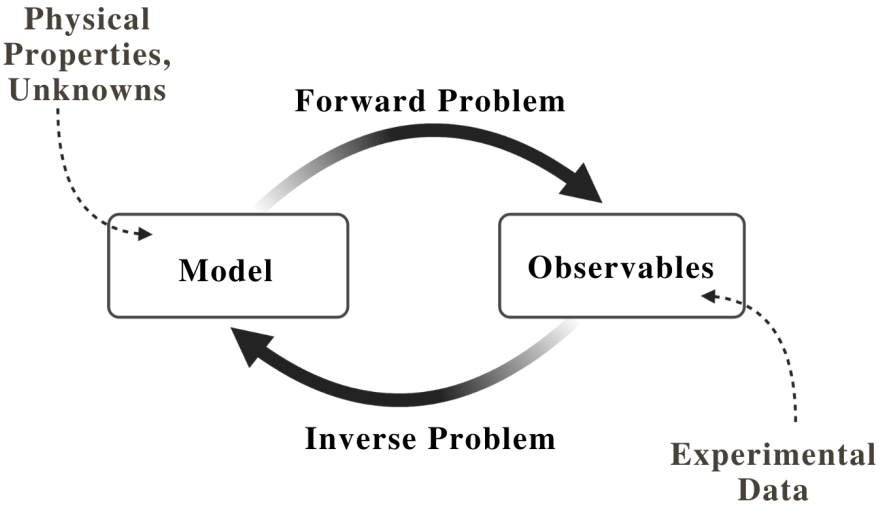

Figure 1: Inverse problems in relation to a forward problems

A common process to solve an inverse problem is to repeatedly solve the forward problem using estimates for any unknown parameters until the model's output is "close enough" to the experimental data. From there, physical properties can be

determined and the model with the closest output to the observables is deemed to be the best fit.
Inverse problems are commonly more complex. For instance, forward problems and solutions typically have a one-to-one relationship, i.e. one problem brings one solution. However, inverse problems usually have a one-to-many relationship, meaning often there are various parameters that can fit the problem. Thus, further analysis on the values would be required to decide which solution is optimal. Additionally, there may not be a solution that exists at all, though, if there is a solution, it could be unstable [12].

1.3.2 Computational Experimental Design

Different experimental designs aimed at parameter inference for the same target parameter can lead to different levels of uncertainty in estimates, and can even lead to different conclusions [13]. The area of optimal experimental design [14, 15, 16] aims to determine the best choice of design and observation types for a given goal. This can be considered an extension of inverse problems theory, where here some degree of choice exists in which experimental data to collect.

The experiment set-up and what it collects has an indirect relationship with the quality of parameter estimations. Figure 2 shows this relationship.

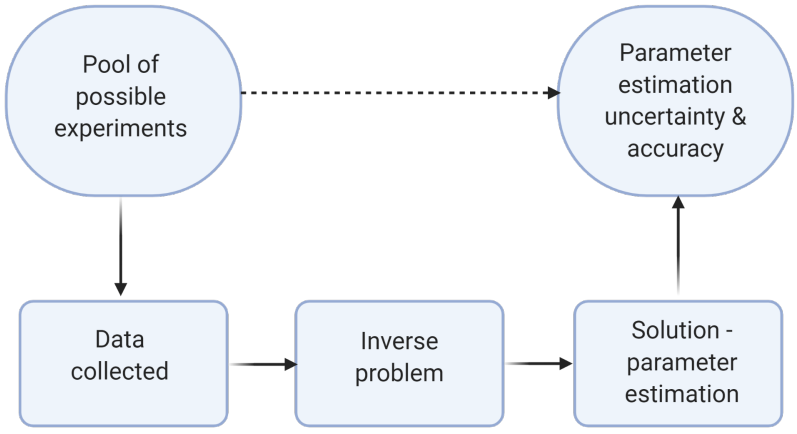

Figure 2: Relationship of experiments to parameter estimates

A particular design will yield a specific parameter estimation. This value may or may not be equal to other parameter estimations from differing experiments but will likely have a different magnitude of uncertainty associated with it.

2 Solving the Forward Problem

2.1 Heat Equation and Conditions

To solve Fourier's partial differential equation (PDE) specified in Section 1.2, conditions must be defined. These are illustrated in Equations 4 and 5 as the boundary and initial conditions, respectively. The conditions specified were used throughout the entirety of the project:

$$u\left(0,t\right)=T, \qquad \frac{\partial u}{\partial x}\left(L,t\right)=0, \tag{4}$$

$$u\left(x,0\right)=T_{\text{ambient}}, \tag{5}$$

where, T is the temperature being applied to the model, L is the length of the model and T_{ambient} is the ambient temperature. The first boundary condition at the beginning of the model ($x = 0$) is referred to as a Dirichlet condition as it specifies temperature. Whereas, the second boundary condition ($x = L$) is a Neumann condition as it sets the flux.

The numerical methods used to solve the equation include the Finite Difference (FD) method and the Finite Element Method (FEM). Each have their relative advantages, however, FD was initially implemented due to its simplicity while FEM was later adopted as it is more robust to model changes. Both solvers were validated against known working solvers and further validated against each other.

2.2 Finite Difference Method

Finite differences solves the PDE by approximating the equation using the Taylor series shown in Equation 6:

$$f(x)=\sum_{n=0}^{\infty}\frac{f^{(n)}(x_0)}{n!}(x-x_0)^n. \tag{6}$$

Implicit or explicit schemes can be derived from considering different Taylor series expansions about x_i. Each scheme has its respective trade offs. Explicit methods are easier to implement and come at a lower computational cost compared to implicit methods. Although, explicit methods have conditionally stability, meaning the solution may not converge, whereas implicit methods do not. A deeper review of the

methods is discussed in section 2.2.1.
Here, an explicit finite difference method was coded to solve the heat equation. A full derivation of the method can be found in Appendix A. The final stencil derived is Equation 7:

$$\frac{D\Delta t}{(\Delta x)^2}(u_{i+1}^n - 2u_i^n + u_{i-1}^n) - u_i^{n+1} + u_i^n = 0, \tag{7}$$

where the superscripts and subscripts represent time and spatial steps in the mesh, respectively. Equation 7 is then rearranged for u_i^{n+1} as all other quantities are known. In this way, the stencil can be applied iteratively to the mesh defined.
For validation, the results were then compared against an equivalent working explicit finite differences method.

It is noted, the classic explicit finite difference scheme needed to be adapted to handle a Neumann condition. This was done by introducing *ghost points* outside of the domain at $L + \Delta x$ (where $x = L$ is the endpoint of the mesh). The ghost points took the values of the $L - \Delta x$ points. That way, the application of the explicit scheme at a boundary point $i = L$ will be correct and guarantee that the solution is compatible with the boundary condition $\frac{\partial u}{\partial x} = 0$.

2.2.1 Comparison of Explicit and Implicit Methods

Both explicit and implicit methods have their respective trade offs. Explicit methods are easier to implement and come at a lower computational cost. However, explicit methods only have conditional stability. The numerical solution is guaranteed to converge only if Equation 8 is satisfied:

$$0 < r = \frac{D\Delta t}{(\Delta x)^2} \leq \frac{1}{2}. \tag{8}$$

Given a high thermal diffusivity, a small time step must be used to satisfy Equation 8. The additional computational cost from smaller time steps could bring explicit methods to be as computationally expensive as implicit methods. For this reason, implicit methods may be of more use.
Implicit methods also have drawbacks. In general, implicit methods come at a greater computational cost compared to an explicit method. However, the solution has unconditional stability meaning a larger time step could be used. Nonetheless, the solution's numerical accuracy depends on r. Hence, it isn't clear which method would be optimal in every situation. Each method should be examined and used based on

the respective problem.

2.2.2 FD Validation

To ensure the created solver works correctly, the solution was compared against a validated explicit finite difference solver. Using identical boundary and initial conditions, the solution was obtained from both the implemented FD solver and the known working explicit FD solver [1, 2]. The results are shown below in Figure 3.

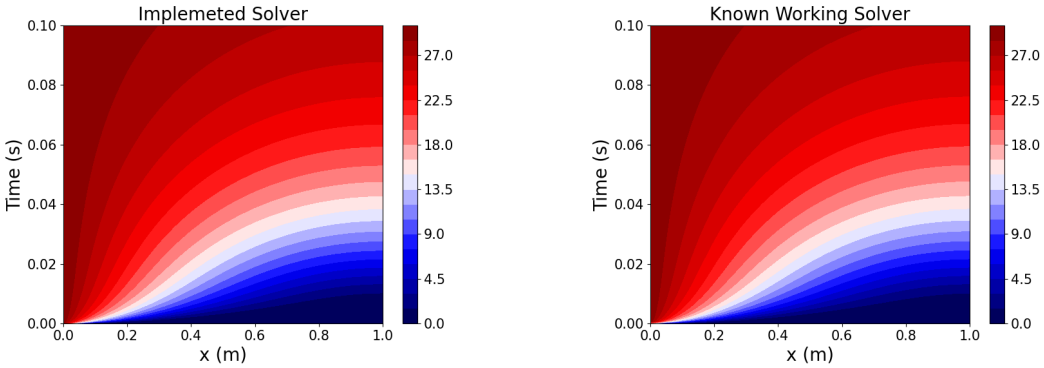

(a) Implemented Solver (b) Known Working Solver

Figure 3: FD validation: comparison of solutions

Although graphs are difficult to accurately compare - it is clear both (a) and (b) are similar in nature. To grasp a better comparison, the differences were quantified by calculating the mean absolute errors (mae) and the root mean squared errors (rmse) between solutions. These values are shown in Table 1.

	Error
mae	3.11E-03
rmse	5.58E-02

Table 1: FD validation: error comparison

Both error values show adequate magnitudes. The mae shows overall, the difference between the validated and implemented solver is small. The rmse shows there are likely no areas with large magnitudes of differences. Therefore, it is likely the implemented solver is behaving as expected.

2.3 Finite Element Method

The finite element method was implemented as it is able to handle arbitrary diffusivity functions with more ease compared to the finite differences solver. FEM can more easily handle Neumann conditions as the solver negates the need for *ghost points* or other additional steps.
In the present context, FEM leads to solve Equation 9 [17]:

$$\frac{d}{dt}\mathbf{M}\boldsymbol{\alpha}(t) = -\mathbf{K}\boldsymbol{\alpha}(t) + \mathbf{q}, \tag{9}$$

where $\mathbf{K}$ and $\mathbf{M}$ are referred to as the *stiffness matrix* and *mass matrix*, respectively. Here, $\boldsymbol{\alpha}(t)$ varies with time only (constant in space). $\mathbf{q}$ is a combination of the forcing term and boundary conditions.

Full details of the FEM formulation can be found in [18] or [19]; however, the basic FEM approach can be summarised in four steps:

1. Form the residual equation
2. Reduce the order of the equation by using integration by parts
3. Introduce interpolating basis functions the basis functions & introduce the weighting function
4. Transform to the element coordinate system where necessary

The basis functions used were piecewise linear. Additionally, although FEM is well-known for its ability to handle irregular shapes, the element space specified was regular. Hence, the distance between each node was constant.

Figure 4 is an example FEM solution and is also the type of distribution expected of a real one layer experiment.

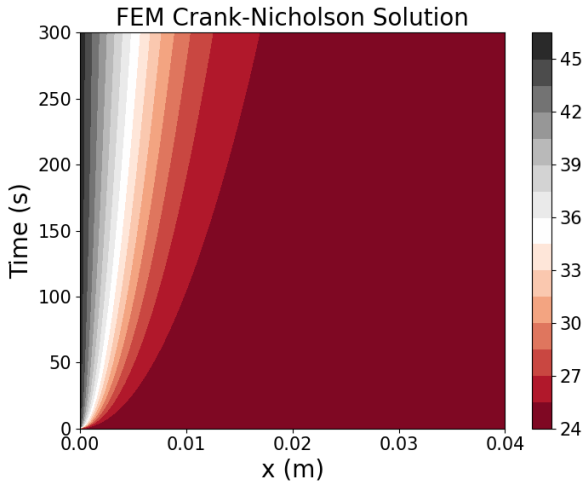

Figure 4: Finite element method solution

The solver in Figure 4 uses the Crank-Nicholson method which solves the time varying component of the PDE ($\boldsymbol{\alpha}(t)$) with central differencing. Hence, to solve for ($\boldsymbol{\alpha}(t + \Delta t)$) at each step, Equation 10 is used:

$$\mathbf{M}\frac{\boldsymbol{\alpha}(t+\Delta t) - \boldsymbol{\alpha}(t)}{\Delta t} + \mathbf{K}[\theta\boldsymbol{\alpha}(t+\Delta t) + (1-\theta)\boldsymbol{\alpha}(t)] = \mathbf{K}\boldsymbol{\alpha}_{\infty} \qquad 0 \leq \theta \leq 1. \quad (10)$$

To implement the Crank-Nicholson method θ is set to $\frac{1}{2}$. The other methods that can be used to handle $\boldsymbol{\alpha}(t)$ include the forward Euler (explicit, $\theta = 0$) or the backward Euler (implicit, $\theta = 1$). All three methods can be used in the FEM code by changing the θ value.

2.3.1 FEM Validation

The FEM code was validated against the semi-analytical solver Simpson et al. (written in MATLAB) used in their 2018 study [3]. Both models were run with identical arbitrary parameters and quantities. A comparison of these models is shown in Figure 5.

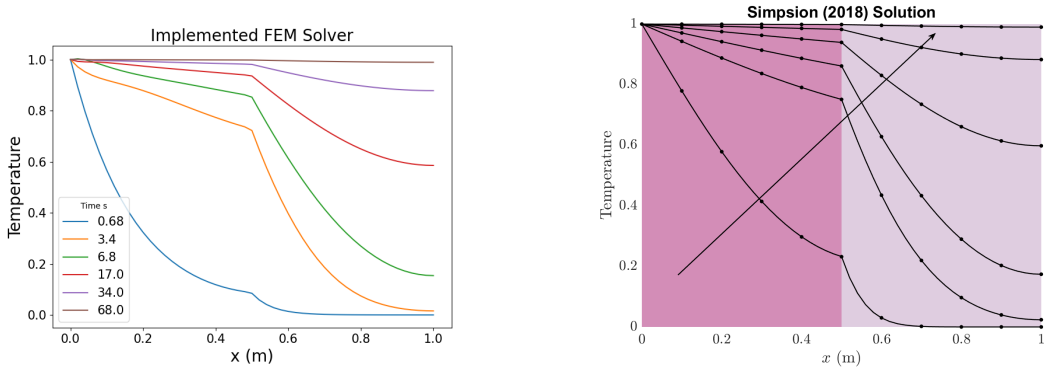

(a) Implemented Solver (b) Known Working Solver

Figure 5: FEM validation: comparison of solutions

There are small differences which may be expected given the Simpson solver is semi-analytic as opposed to FEM which is entirely numerical. In addition, although the input parameters are the same, the time stamps used for comparison here are not identical due to the nature of the MATLAB code (difficult to perfectly adjust). Therefore, FEM was further validated against the FD solver written previously. Identical mathematical models were solved using both FD and FEM, the solutions are shown in Figure 6.

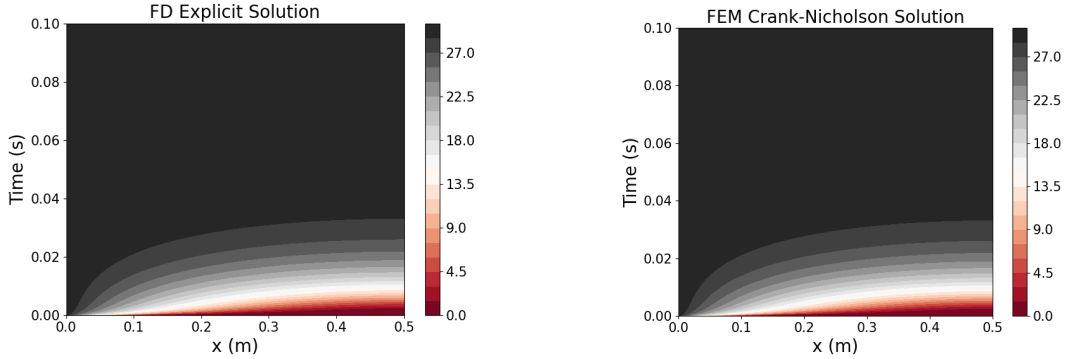

(a) Finite Difference Solver (b) Finite Element Solver

Figure 6: FEM validation: FD comparison

3 Solving the Inverse Problem

To determine the value of parameters given data, also known as model calibration, inverse modelling typically uses numerical methods. A common method of model calibration seeks to find a parameter estimate, ϕ^*, by minimising some objective function, $S(\phi)$, measuring the fit of the model to observations given the parameter [12].

Here, the inverse problem is solved by constructing an objective function comparing the observed data to the model solution given a parameter. This objective function is then used as an input to an optimisation algorithm which iteratively solves the forward problem using various values for the thermal diffusivity. The solution of each forward problem is then compared against the observables until an optimum or satisfactory parameter is found.

For verification, validation, and to better understand the problem posed, synthetic data was evaluated before the experimental data. The analysis using real data is described in Section 5.

3.1 Parameter Recovery

To solve the posed non-linear optimisation problem, SciPy's least-squares function was implemented [20]. For a given set of parameter values and model, $f(x;\phi)$ the prediction of the model is $y_i = f(x_i;\phi)$. However, this prediction will have error compared to noisy (real or synthetic) data and thus, a misfit (or residuals) can be calculated as $\bar{y}_i - y_i$. Minimising the sum of squared residuals leads to an objective function of the form:

$$S(\phi) = \sum_{i=1}^{N} (\bar{y}_i - y_i)^2. \tag{11}$$

SciPy's least-squares takes the residuals as an input by having them as the objective function's output. The objective function solves the forward problem by calling the FEM solver with the initial ϕ as an input (FEM(ϕ)). The output of FEM(ϕ) is the temperature distribution of the same model the experiment mirrors. The residuals are then computed (experimental data minus FEM(ϕ) output) and passed on to the least-squares function. Once a stopping criteria has been satisfied, the corresponding parameter is returned. A high-level process is portrayed in Figure 7.

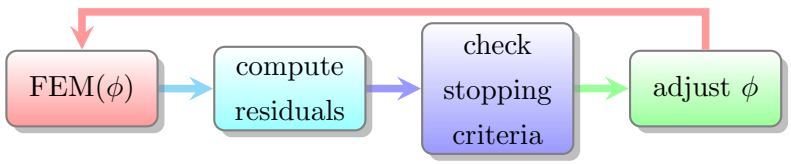

Figure 7: Parameter recovery process

It is noted, the models were also run using FD to ensure the solver was behaving as it should. No alarming differences between the runs were found.

3.2 One Layer

Synthetic data was fabricated to test the parameter recovery approach. The data was created by solving FEM, taking the temperature distribution and cutting it down to the number of locations the experiment requires. Noise was then added to this temperature distribution. The standard deviation of the noise was 0.3 (and mean = 0) as this was the expected noise for real experiments.

First, a one layer model was explored. Hence, the thermal diffusivity used to fabricate the synthetic data was a constant.
Four synthetic experiments were undertaken all with varying quantities of data being "measured" at all time stamps: measuring temperature at one location (one probe); two locations (two probe); three locations (three probe), and; one experiment assuming the temperature was known at all locations (all points).
The inputted diffusivity used was 9.09E-08 (this was a somewhat arbitrary value, in that, it was similar to that expected from the real experiments but not the exact parameter). Only the *all points* model was able to recover this parameter exactly. The one, two and three probe models returned 9.12E-08, 9.08E-08 and 8.98E-08, respectively.

3.3 Two Layer

To model a multi-layer phantom, a noncontinuous piecewise function for the diffusivities was used. A graphical representation of this equation is shown in Figure 8.

Where D_1 and D_2 are some specified diffusivities for the first and second layer, respectively. Continuous functions were also considered, however, it was concluded piece-wise functions would better depict the skin structure. The FEM solver is able to handle any reasonable function type as an input for diffusivity. The function used in the FEM code can be found in Appendix B. The code shown handles up to three layers as every "interface" variable's default value is larger than any domain range.

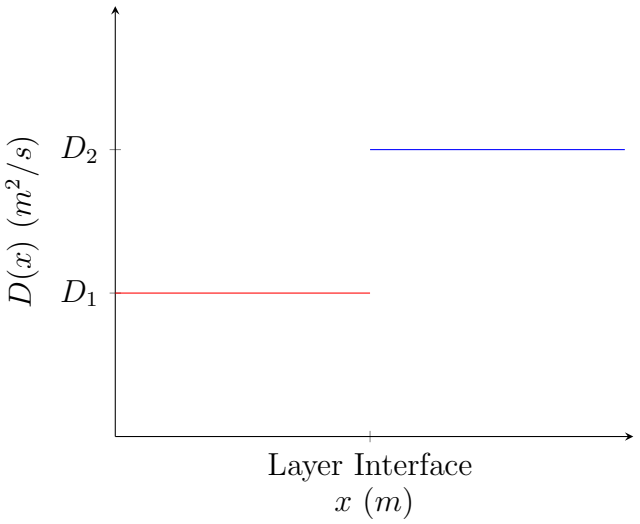

Figure 8: Two layer diffusivity function

Nevertheless, the function can be altered to fit various diffusivity functions with respect to space. Therefore, if in the future, a function besides piece-wise is deemed to be more suitable, the changes to the code would be minor.

The inputted diffusivity values, D_1 and D_2 were 9.09E-08 and 7.68E-07. Two synthetic experiments were performed: *two probes* (one probe in each layer to mimic a probable real experiment) and *all probes*. Again, the *all probes* was able to recover the inputted D_1 value to the same degree. However, the second layer diffusivity parameter recovered was 6.76E-07. The *two probes* experiment recovered parameters of 9.15E-08 and 3.06E-06 for D_1 and D_2, respectively.

3.4 Multiple Layers

Additional layers better replicate skin's inhomogeneous nature. To test the functionality and feasibility of additional layers, a three layer model was investigated. It is noted the implemented FEM code is built to handle however many layers required with minimal adaption needed. A similar function to that in Figure 8 was adopted but with three diffusivity values instead.

Two data sets were run: *three probes* (one probe in each layer) and *all points*. The inputted thermal diffusivities were: $D_1 = 9.09\text{E-}08$, $D_2 = 7.68\text{E-}07$, $D_3 = 6.00\text{E-}06$. Both the *three probes* and *all points* models recovered D_1 perfectly. The *three probes* model recovered D_2 to be 2.75E-07 and the *all points* model recovered it to be 8.10E-07. The diffusivity for the third layer, D_3, estimation was found to be anywhere from the E-09 (1.69E-09 for *all points*) range to the E-07 (1.93E-07 for *three probes*) range, despite the inputted value being in the order of E-06.

In addition to single point estimates, the uncertainty associated with these can be quantified to enable better conclusions in the presence of noisy data. The uncertainty associated with estimates also provides key additional information for experimentalists concerning which designs provide the most reliable estimates.

4 Uncertainty and Design

4.1 Linear Uncertainty

Linear uncertainty was implemented by calculating the 95% confidence interval of each experiment's run.

The Jacobian of the model's output with respect to the model's input (an output of the least-squares function) was manipulated to calculate the covariance matrix of the estimates using [12]:

$$\text{Cov}(\phi^*) = \sigma^2 (J^T \cdot J)^{-1}. \tag{12}$$

In Equation 12, σ is the standard deviation of the data itself if the experiment was real or, for synthetic data, the standard deviation used to fabricate the noise.

4.2 Likelihood Profiling

The likelihood profile was computed by considering the objective function as the log likelihood. Hence, probability density function equation used is depicted in Equation 13 [12]:

$$p(y^0|\phi) = \frac{1}{\sqrt{2\pi\sigma^2}} e^{\left(-\frac{(FEM(\phi)-y^0)^2}{2\sigma^2}\right)}. \tag{13}$$

The likelihood value for each evaluated parameter was divided by the maximum likelihood estimate (MLE) across all considered parameters. This gives the relative likelihood function, which can be thresholded to form confidence intervals; appropriate thresholds are determined based on an approximate chi-squared sampling distribution [21]. Profile likelihood has also been shown to provide an effective tool for carrying out parameter identifiability analysis [22].

Where the variance used in the least-squares function is constant for all data points, the $\frac{1}{\sqrt{2\pi\sigma^2}}$ term can be ignored as the ratio will always be equal to 1. The likelihood function is proportional to the probability density, though considered as a function of the parameter for fixed data. Hence, the likelihood function is proportional to:

$$f(\phi|y^0) \propto e^{\left(-\frac{(FEM(\phi)-y^0)^2}{2\sigma^2}\right)}. \tag{14}$$

Accordingly, the resulting likelihood is stated in Equation 15:

$$\mathcal{L}(\boldsymbol{\phi}|y^0) = \frac{f(\phi|y^0)}{f(\hat{\boldsymbol{\phi}}|y^0)}, \tag{15}$$

where, $\hat{\boldsymbol{\phi}}$ are the parameters that produce the MLE.

However, if the residuals were too large, $f(\phi|y^0)$ approximates to zero. To overcome

this, Equation 15 was rearranged to Equation 16:

$$\mathcal{L}(\boldsymbol{\phi}|y^0) = e^{-\frac{1}{2\sigma^2}\left((FEM(\phi)-y^0)^2-(FEM(\hat{\boldsymbol{\phi}})-y^0)^2\right)}. \tag{16}$$

For individual parameters, the likelihood profile uses the parameter from Equation 17:

$$\underset{\phi}{\operatorname{argmax}}\, f(\phi|y^0) = e^{\left(-\frac{(FEM(\phi)-y^0)^2}{2\sigma^2}\right)}. \tag{17}$$

Confidence intervals can also be constructed based on the likelihoods. Therefore, where linear uncertainty qualification was difficult, the method shown in Equation 18 was used [21].

$$\left\{\boldsymbol{\phi}, \frac{\mathcal{L}(\boldsymbol{\phi}|y^0)}{\mathcal{L}(\hat{\boldsymbol{\phi}}|y^0)} > 0.05\right\}. \tag{18}$$

The threshold of 0.05 is for joint inference for exactly two parameters only (threshold is dependent on the number of parameters [12]). When considering likelihoods targeting individual parameters, the threshold becomes 0.15 and often produces more precise values than individual intervals based on projections of joint confidence regions, while maintaining appropriate coverage [12, 21].

A range of 41 and 61 different values were used for D_1 and D_2, respectively when determining individual likelihood profiles (D_3 took on 61 values for synthetic data). The number of diffusivities were not equal as D_2 did not plateau at 41 in some cases (visible in Figure 10). Therefore, to investigate two parameters, 2501 (61×41) distinct pairs were tested. These sample numbers were consistent across all non-linear uncertainty quantification applications.

4.3 Verification on Synthetic Data

The confidence intervals observed for the same synthetic data from Section 3.1 can be found in Appendix C in Tables 6, 7 and 8 for D_1, D_2 and D_3, respectively.

The confidence interval widths, on average, increased with the layer. The program became more unsure regarding the estimations of lower level layers. This is despite the number of measuring probes and type of experiment (one, two, or three layers). Furthermore, it was not surprising to note, the more measuring probes instilled lower uncertainty in the estimate - as reflected by the interval widths.

Using synthetic data, the likelihood profiles were computed for one, two and three layer models. Figure 9 shows the one layer model simulating three probes. Various numbers of probes were also graphed (one, two, three and all points known) and all showed identical trends.

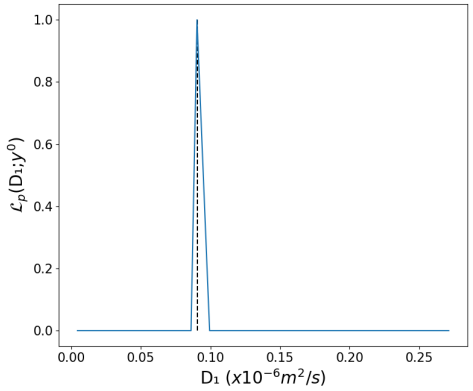

It's clear in Figure 9, the diffusivity in a one layer model is well identified. Therefore, there shouldn't be any identifiability issues when attempting to recover the diffusivity in the real experiments. However, different conclusions were made when investigating a two or three layer model.

Figure 9: One layer synthetic data likelihood profile

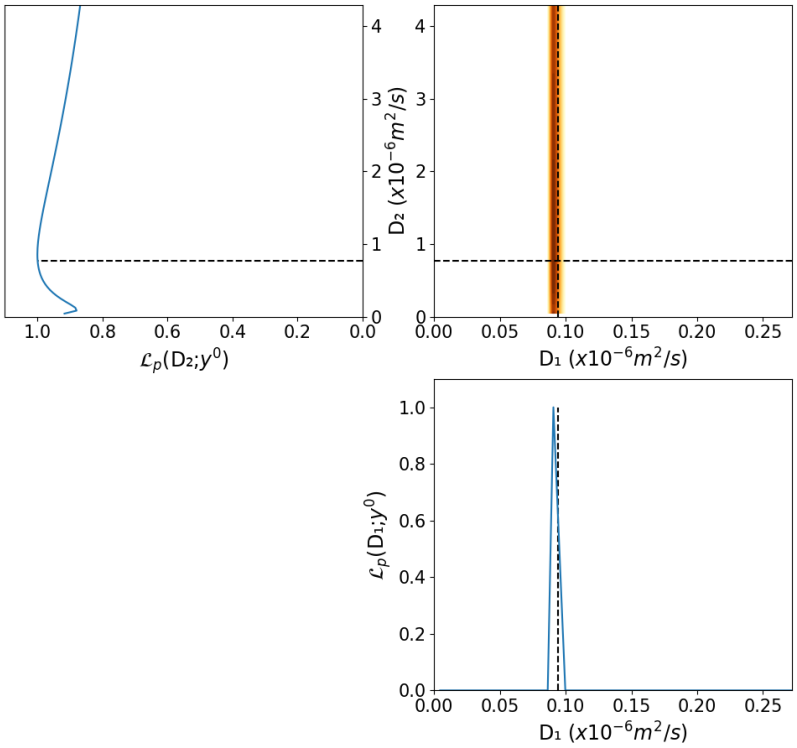

Figure 10: Two layer synthetic data likelihood

The black dashed lines shows the *calculated* diffusivities. The contour plots show the likelihood of that parameter pair being the "true" values where a darker region

represents a higher likelihood. The single profiles are essentially "side views" of this contour plot where only one parameter is considered. This structure is used for all likelihood profile plots.

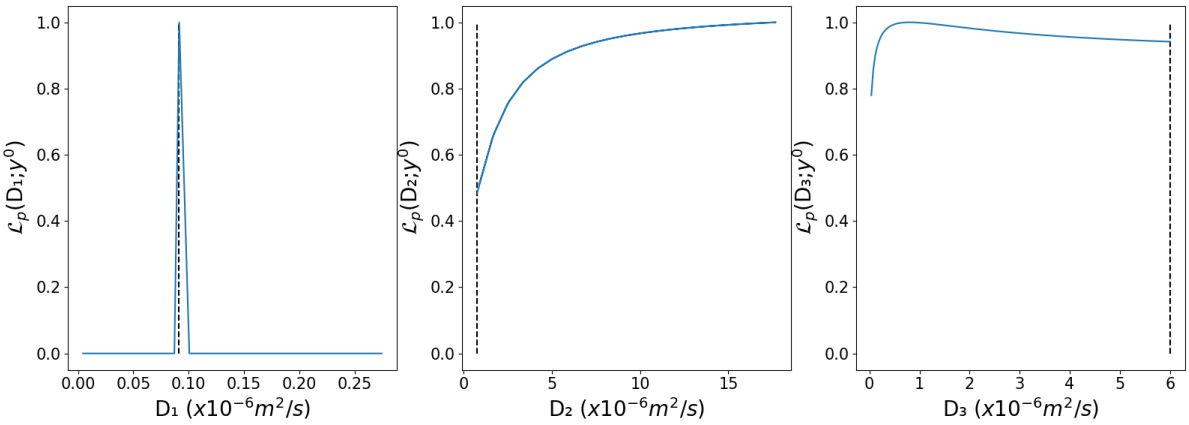

Figure 11: Three layer synthetic data likelihood

As shown in Figures 10 and, 11 although the inputted parameters are captured under the curve and show a high likelihood of being the *true* parameters, the exact nature of the diffusivity in the second and third layer cannot be determined. This indicates potential identifiability issues.

4.4 Synthetic Data Findings

Measuring closer to the end of the model (@$x = L$, where $x = 0$ is the heat source location) produced more accurate results than if the data was collected closer to/at the heat source (see [23], Section 1).This is possibly due to the fact the boundary condition is the same for all parameters considered and, therefore, different models only begin to diverge (in terms of temperature predictions) away from this common condition.

Diffusivity parameters for layers beyond the first cannot be accurately recovered, if at all. The synthetic data suggested these parameters have identifiability issues. Similar results have been found by Simpson et al. in 2018 [3]. However, the first layer diffusivity should be able to be recovered reasonably well in any tested situation. Finally, the addition of measuring probes results in smaller confidence interval widths.

5 Application to Real Experiments

5.1 Experimental Thermal Diffusivity

Experiments to measure the individual components of thermal diffusivity were carried out. Details of these experiment's can be found in Anthony Zemke's report [4]. Equation 2 was then used to calculate what was assumed to be the thermal diffusivities for 1% and 5% agar gel concentration phantom discs. The 1% solution was used throughout any one layer experiment and as the bottom layer for any two layer experiment. Details of these values is shown in Table 2.

	c	λ	ρ	D
Gel %	(J/kg·K)	(W/m·K)	(kg/m^3)	(m^2/s)$\times 10^{-8}$
1.0	7806 ± 582	0.674 ± 0.050	918 ± 2	9.41 ± 1.43
5.0	4091 ± 232	0.569 ± 0.021	981 ± 2	14.18 ± 1.22

Table 2: Experimental thermal diffusivity values
Extracted from [4]. c = Specific Heat Capacity. λ = Thermal Conductivity. ρ = Density. D = Thermal Diffusivity.

5.2 Description of Experiments and Data

The general experimental design consisted of a heating mat placed on top of a phantom disc made from varying concentrations of agar gel. The various agar gel concentrations result in different thermal diffusivities and, therefore, act as distinct skin layers.

The heating mat was not directly in contact with the gel phantom, instead, a highly conducting aluminium disc was between the two. A probe (T1 in Figure 12) was placed either in the middle of this metal disc - referred to as the unmodified experiment - or, between the disc and the phantom - the modified experiment. The temperature at this probe was used as the boundary condition for the forward problem.

Six different experiments were conducted in total with various combinations of the following factors: the number of probes measuring temperature; the number of agar gel layers used in the model, and; whether the experiment was modified or unmodified. All experiments are shown in Figure 12. For further details, see [4].

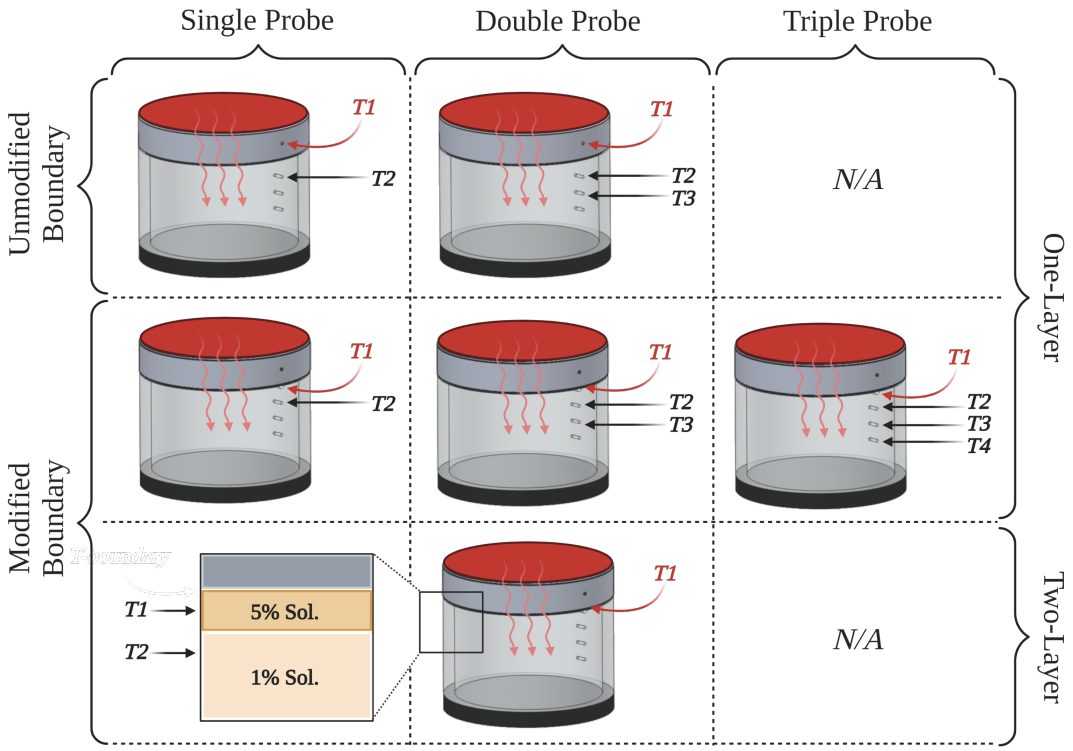

Figure 12: Agar gel phantom experiments preformed
Extracted from [4].

The modified and unmodified experiments measure the exact temperature being applied to the model at different locations. After reviewing the initial set-up (unmodified, probe places within the highly conductive disc), the temperature at the bottom of the disc was examined and compared to the temperature measurements from within the aluminium disc. There was a difference of, on average, $10°C$. Hence, the assumption that the aluminium disc was conductive enough that this difference in measuring location was not relevant could not be justified. Consequently, It became clear moving the boundary probe to be in direct contact with the disc plane exposed to the gel would provide a more useful model as this better represented the *true* boundary condition. Thus, the final experimental set-up (modified) was developed.

5.2.1 Boundary and Initial Conditions

The initial condition used was an average of temperature measurements of all the probes within the phantom at $t = 0$. It was clear if the experiment was a single probe, the initial condition is prone to more error given the value cannot be averaged. For all experiments however, all temperature values preceding the start of the experiment

were examined to ensure they were roughly constant.

The boundary conditions, specifically the side of the heat source, however, were more difficult to accurately define. The heating mat could only be kept at a constant flux, meaning a constant temperature could not be ensured. Hence, adjusting the heat source condition from a Dirichlet condition to a Neumann condition was an option. Yet, after graphing the measurements from the boundary probe (example shown in Figure 13), it became apparent neither the flux nor the temperature were constant.

Therefore, a time-dependent Dirichlet condition was used in place of the previous constant value. The constant was clearly not representative of the experiments. To reduce model error, the measurements from $T1$ (Figure 12) were used directly as the $x = 0$ boundary condition. The impact of the choice of boundary conditions is considered further in Section 5.3.

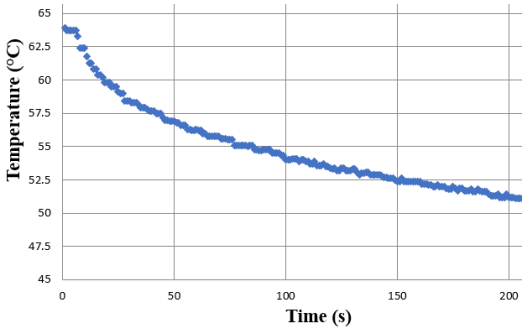

Figure 13: Boundary temperature of one layer, one probe experiment

5.2.2 General Model Properties

Values listed apply to all experiments unless stated otherwise.

- Number of experiment repeats: 4 (5 for unmodified one probe, one layer experiments)
- Phantom disc length: 6.0 cm (4.0 cm for unmodified one probe, one layer experiments; 6.2 cm for two layer experiments)
- Probe 1 location: 1.1 cm deep (1.2 cm for two layer experiments; 2.1 cm for both one probe, one layer experiments)
- Probe 2 location (where applicable): 2.1 cm deep (2.2 cm for two layer experiments)
- Probe 3 location (where applicable): 3.1 cm deep (3.2 cm for two layer experiments)
- Experiment run time: 5 minutes (10 minutes for three probe experiments)

- Interface location (two layer experiments only): 2.1 cm deep

The standard deviation used throughout the estimation uncertainty quantification was set to 0.3. This value was determined by taking the standard deviation of multiple idle probes for, more or less, 10 minutes each. The average calculated standard deviation was deemed to be approximately 0.27. However, the value of 0.3 was used to add a small buffer and ensure the standard deviation was not being underestimated.

The initial guess used for the least-squares solver was 14.79E-08. This value is the thermal diffusivity of water at ambient temperature (26.9°C in this case) [24]. This particular diffusivity was used as it is known the phantom's thermal diffusivity should be reasonably close to this value. Therefore, this decreases the chance of the optimisation solver landing in an undesired local minimum.

5.3 Results and Discussion

A full list of the one layer recovered diffusivity values can be found in Appendix D as the column D_{rec}.

Figure 14 illustrates the common parameter recovery trend across all experimental runs. Specifically, this figure shows data and model fit for a one-layer, two-probe experiment. Two sets of coloured lines are shown - each set is at a different probe location (locations are specified in Section 5.2.2). The green sporadic line is the experimental data - what the program is attempting to fit. The blue line is the resulting model fit. The red line is what the model would look like with the diffusivity values calculated from direct measurements of gel thermal properties carried out by Anthony Zemke [4].

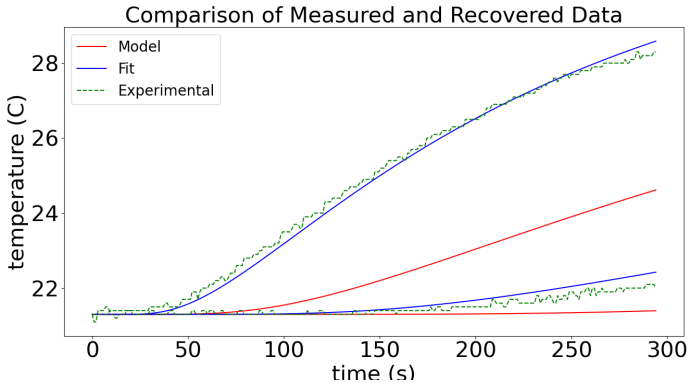

Figure 14: Parameter recovery: one layer, two probe experiment

It's the clear that although the "true" model and the fitted model are far apart, the model can fit the data reasonably well when using different diffusitivities than those determined by direct measurements. It's possible a number of factors are playing a part in this mismatch. The mathematical model may be missing terms or influential aspects that haven't been considered. Another possibility is the experiments to directly calculate the diffusivity from component properties may be missing important terms and/or factors. Furthermore, these experiments may be subject to systematic measurement errors.

From Table 9, the modified and unmodified show significantly different results. Therefore, a short investigation regarding the importance of accurate boundary conditions was undertaken. Synthetic data was fabricated using various Dirichlet boundary conditions including constants, real experimental boundary probe temperature values, and time varying conditions. This synthetic data was used in an attempt to recover the parameter using a model involving a different boundary condition than that used to fabricate the data. These results were then compared against the synthetic data parameter recoveries in Section 3.1. It was found the boundary condition plays a large role in the model's ability to recover the parameter. If the computational and experimental model do not have the same boundary condition, the model struggles to accurately and consistently produce a *good* estimate of the parameter originally used to manufacture the data.

The linear uncertainty techniques discussed in Section 4.1 were also applied. The average width of the confidence intervals was calculated. It is important to note however, that there was no interval overlap across and within any experimental designs - this is again suggestive of model misspecification. Furthermore, when attempting to calculate the intervals for a two layer model, it was found the Jacobian was often singular for the diffusivity of the second layer. Rather than a model misspecification issue, this is consistent with the synthetic data results in the previous section, and indicates a lack of enough information (as opposed to biased or incorrect information) from the given experiments. Therefore, applying this specific method became difficult. Subsequently, the confidence intervals for these experiments were based on profile likelihood methods, discussed later in this section.

One layer confidence intervals and the range of diffusivities that were recovered from the experiment runs are displayed in Table 3.

Experiment	D_{rec} Range	Average Width
One Probe Unmodified	[8.61E-08, 2.29E-07]	3.84E-09
One Probe Modified	[1.35E-07, 2.74E-07]	2.72E-09
Two Probe Unmodified	[6.36E-08, 1.17E-07]	2.60E-10
Two Probe Modified	[2.10E-07, 2.32E-07]	5.13E-10
Three Probe Modified	[1.74E-07, 2.16E-07]	1.40E-10

Table 3: D_1 average 95% confidence interval widths for real one layer experiments

All values are somewhat similar but it is clear the width is the smallest for the three probe modified experiment while also maintaining close proximity to the calculated diffusivity. Additionally, when converting to likelihood values and visualising the distribution, all experiments produced plots of an identical shape to that from the one layer synthetic data model in Figure 9. This indicates the model did not have trouble locating the parameter, suggesting evidence for strong D_1 identifiability.

On the other hand, the opposite was found for the second layer diffusivity. For the two layer experiments, first confidence intervals were constructed from the relative likelihood values. However, the interval for D_1 was found to be extremely small, therefore, the point at $\mathcal{L}(D_1|y^0) = 1.0$ and the two neighbouring $\mathcal{L}(D_1|y^0) = 0.0$ points were interpolated using SciPy's *interp1d* with the "quadratic" method (cubic was preferred but requires at least four points to establish the spline). The intersections of this function and $\mathcal{L}(D_1|y^0) = 0.15$ were found and given in Table 4 as the lower and upper bounds.

	Lower Bound	Recovered D_1	Upper Bound	Interval Width
Exp 1	2.13E-07	2.26E-07	2.39E-07	2.60E-08
Exp 2	1.57E-07	1.70E-07	1.83E-07	2.60E-08
Exp 3	2.15E-07	2.28E-07	2.41E-07	2.60E-08
Exp 4	1.81E-07	1.94E-07	2.07E-07	2.60E-08

Table 4: D_1 95% two layer experiment confidence intervals
Exp = Experiment run

All widths for D_1 were approximately equal possibly due to the interpolation method used. Nevertheless, D_1 showed strong identifiability in all runs.

	Lower Bound	Recovered D_2	*MLE* D_2	Upper Bound	Interval Width
Exp 1	4.77E-06	7.14E-06	7.14E-06	1.21E-05	7.37E-06
Exp 2	2.12E-06	4.93E-06	4.93E-06	2.37E-05	2.16E-05
Exp 3	2.51E-05	1.73E-04	8.67E-04	-	-
Exp 4	6.36E-05	2.65E-04	1.33E-03	-	-

Table 5: D_2 95% two layer experiment confidence intervals

The last two experiment runs have no upper bound as the interval was effectively infinity on one side. This implied the parameters were found to be one side identifiable. Interestingly, for these runs, the diffusivity value that produced the *MLE* was not the same parameter that was recovered (although it was *relatively* nearby). It could be that the least-squares solver landed in a local minima, was constrained in the parameter space.

The two layer model's likelihood profiles for experiments 1 & 2 are presented in Figure 15.

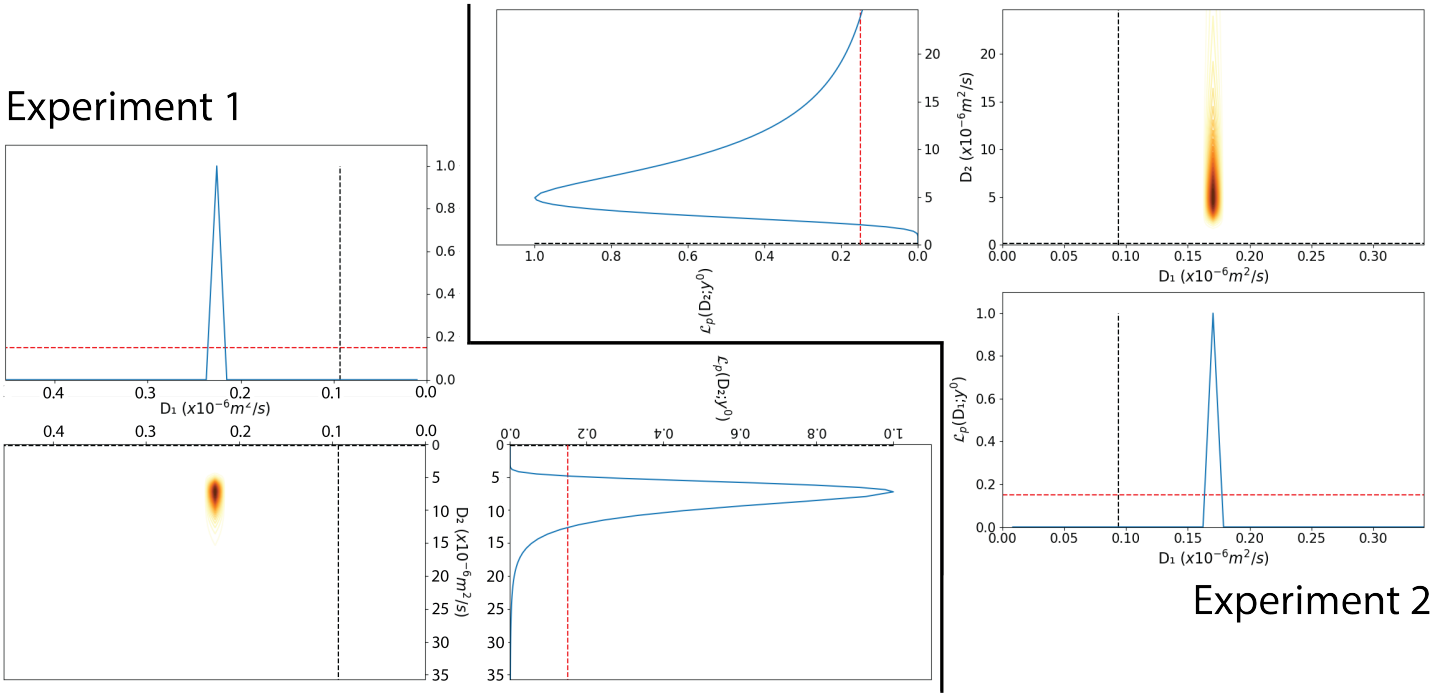

Figure 15: Two layer Experiment 1 & 2: likelihood profiles

The bold black line separates each experiment run where the first experiment is on the left side of the line and the second, on the right. The black dashed lines

are the *experimentally calculated* diffusivities (as mentioned earlier), however, the *experimentally calculated* D_2 was small relative to the specified D_2 values. Hence, the black dashed line for D_2 are not perfectly visible. The red dashed lines show the 15% relative likelihood threshold and, therefore, indicate an approximate 95% confidence interval based on a chi-square calibration for each *individual* profile [21]. Experiment 1 suggests D_2, although having a range of viable solutions, can be well identified. Nevertheless, this implication stood alone as the other 3 experiment runs showed otherwise. Experiment 2 implies D_2 is "weakly" or "one-sided" identified: only a lower bound can be placed on D_2, and there is no upper bound.

Experiment 1's conclusion may have basis as the following experiments were possibly prone to a higher degree of error given the phantom was repeatedly heated and left to cool multiple times by the time of the next experiment. This process could have very well affected the performance and further explain the highly varying results across runs within this single design.

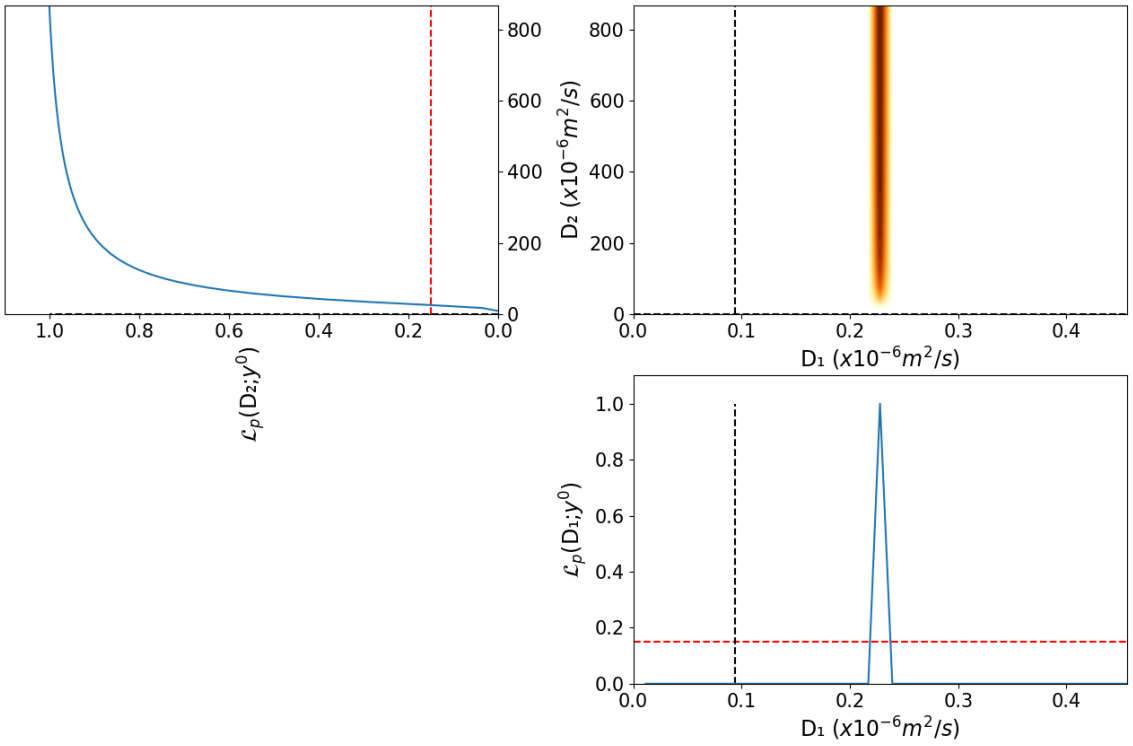

Figure 16: Two layer Experiment 3: likelihood lrofiles

Experiments 3 and 4 produced profile likelihood's of similar shapes therefore, only Experiment 3's profiles are shown (Figure 16), Experiment 4's plots can be found in Appendix D as Figure 17.

From Figure 16 it can be said that the second layer diffusivity value is larger than ≈ 0.1, an upper bound cannot be deduced in any way - meaning the parameter is only "one side identifiable". Similar results have been shown and described in the literature review [5].

Notably, the two dimensional case which worked for synthetic data (i.e. captured the *true* parameter), missed the truth for **all** real data which indicates possible model error (i.e. misspecification) and/or systematic measurement error. The effect of boundary conditions may also play a part in this difference between real and synthetic results - where the boundary conditions were inaccurate, the impact was reflected through the recovered parameter.

5.3.1 Limitations

It was assumed that the temperature being applied to model is known, this assumption may not be justified completely. Although the probe was moved from the middle of the aluminium disc to the bottom in an attempt to more accurately capture this temperature, the boundary probe itself may affect the temperature applied to the model.

Furthermore, in all experiments, it is possible probes may have affected each other as they are only, on average, 1 cm apart. Heat absorbed by one probe (outside of the phantom) likely diffused to the probes around it. These affected probes therefore would have measured temperatures higher than the actual temperature. This could explain all recovered diffusivities being larger than the experimentally observed diffusivity.

The agar phantom model is not isolated in empty space (which the mathematical model represents) but instead enclosed in an acrylic cover. Hence, heat could be lost to this surrounding material. Heat could also be lost in various other points such as the bottom. This contradicts the Neumann boundary condition of zero heat flux at the bottom of the model.

Additionally, a simple diffusion equation may not be correct [25]. It may turn out that a nonlinear diffusion is more appropriate. Furthermore, source terms are also possibly relevant factors that were assumed otherwise.

Finally, because the thermal diffusivity and the heat being applied to the model are both small, knowing the exact locations of the probes is critical. The locations

heavily impact the results, however, they were not perfectly determined in these experiments. The measuring probes appeared to have entered the gel at a slight angle or ended up in a different location than what was intended and therefore, affected the recovered parameter.

6 Conclusions

Through this investigation, it was concluded that a one layer model with a few probes far from the heat source can predict parameters well given systematic and model error is minimal. It was also noted that multi-layered models require further development before any sound conclusion can be drawn regarding their ability to recover thermal diffusivities past the first layer by a burn-to-skin mimicking experiment.

Therefore, while experimentally performing scalds on phantoms with two or more layers isn't out of the question, it may be too difficult to determine the unique thermal diffusivity of each layer (after the first) with accuracy. However, this may only be the case with this project's current methodology and design.

Ultimately, this project has provided a basis for future work and further investigation into the world of burn injuries, skin mimicking phantoms, parameter recovery and uncertainty quantification. Optimistically, the project will enhance understanding of burn injuries and how to experimentally and mathematically model them.

6.1 Future Work

Naturally, a next step would be to conduct and analyse three layered phantoms. Despite what the synthetic data concluded with reference to the third layer diffusivity identifiability issues, investigating a three layer model in conjunction with improved experimental protocols (see [4]) could provide promising results.

Performing experiments to explicitly quantify the possible effects the presence of the probes could have on the results would be useful. If no effect is established, it would rule out possible errors. Thus, this would be a beneficial future exercise. Another possible improvement would be to leave the boundary condition as an unknown and left to be estimated simultaneously. The interface can also be assumed to be an unknown and recovered by the program. This was briefly investigated but eventually

found was associated with many complications. Therefore, analysing the boundary condition in greater depth should have been completed given additional resources.

Taking into account multi-spatial dimensions when solving the forward problem and evaluating the differences in relation to the current model would be useful. It is possible the one spatial dimension assumption cannot be rightly supported. Otherwise, it can be concluded one spatial dimension will suffice and the computational cost of including more cannot be justified by the additional accuracy it brings.

Exploring various uncertainty quantification and optimisation techniques could be of use to validate the results of this project. Particularly, Bayesian uncertainty estimation can be used to construct uncertainty intervals where the Jacobian was found to be singular rather than using the likelihood profiles.
Furthermore, the least-squares function often returned a local minima rather than a global minima. Hence, a metaheuristic optimisation technique could be employed and run for a long period to ensure a *good* solution is found (likely better than a least-squares solution).

Following the synthetic data findings, a weighted least-squares approach should be taken for real data with emphasis being placed on probes measuring temperature further from the boundary. It would be interesting to note whether the parameter estimation improves. This result would immediately provide a starting point regarding the optimal location for the measuring probes.

Lastly, to expand the currently isolated skin model and therefore, better reflect reality, a blood perfusion term should be incorporated into the mathematical model (easily handled by the FEM solver) and by extension, the experiments. Simulating this additional factor could contribute a valuable starting point for their respective experiments in the future.

References

[1] Fu, Rui and Weng, Haoyue and Wenk, Jonathan F. and Martin, Alexandre. Thermomechanical Coupling for Charring Ablators. *Journal of Thermophysics and Heat Transfer*, 32(2):369–379, 2018.

[2] Fu, Rui and Weng, Haoyue and Wenk, Jonathan F. and Martin, Alexandre. Thermal Expansion for Charring Ablative Materials. *Journal of Thermophysics and Heat Transfer*, 34(1):57–65, 2020.

[3] McInerney, Sean and Carr, Elliot J. and Simpson, Matthew J. Parameterising continuum models of heat transfer in heterogeneous living skin using experimental data. *bioRxiv*, page 354563, September 2018. Publisher: Cold Spring Harbor Laboratory Section: New Results.

[4] Zemke, Anthony. Optimal Experimental Design for Understanding Burn Injuries. Technical report, The University of Auckland, October 2020.

[5] Shahin, Marah. Optimal Experimental Design for Understanding Burn Injuries - Literature Review and Statement of Research Intent. Technical report, The University of Auckland, October 2020.

[6] Tintinalli, Judith and Stapczynski, J and Ma, O John and Cline, David and Cydulka, Rita and Meckler, Garth. *Tintinalli's emergency medicine: a comprehensive study guide: a comprehensive study guide*. McGraw Hill Professional, 2010.

[7] Basil A. Pruitt, Steven E. Wolf, and Arthur D. Mason. Chapter 3 - Epidemiological, demographic, and outcome characteristics of burn injury*. In David N. Herndon, editor, *Total Burn Care (Fourth Edition)*, pages 15 – 45.e4. W.B. Saunders, London, Fourth Edition edition, 2012.

[8] Cho, Jiyong and Prasad, Bibin and Kim, Jung Kyung. Near-infrared laser irradiation of a multilayer agar-gel tissue phantom to induce thermal effect of traditional moxibustion. *Journal of Innovative Optical Health Sciences*, 11(06):1850033, August 2018. Publisher: World Scientific Publishing Co.

[9] Narasimhan, TN. Fourier's heat conduction equation: History, influence, and connections. *Reviews of Geophysics*, 37(1):151–172, 1999.

[10] Simpson, Matthew J and McInerney, Sean and Carr, Elliot J and Cuttle, Leila. Quantifying the efficacy of first aid treatments for burn injuries using mathematical modelling and in vivo porcine experiments. *Scientific reports*, 7(1):1–11, 2017.

[11] Bird, R Byron. Transport phenomena. *Appl. Mech. Rev.*, 55(1):R1–R4, 2002.

[12] Aster, Richard C and Borchers, Brian and Thurber, Clifford H. *Parameter estimation and inverse problems*. Elsevier, 2018.

[13] Parker, Andrew and Simpson, Matthew J and Baker, Ruth E. The impact of experimental design choices on parameter inference for models of growing cell colonies. *Royal Society open science*, 5(8):180384, 2018.

[14] Pukelsheim, Friedrich. *Optimal design of experiments*, volume 50. Society for Industrial and Applied Mathematics, 2006.

[15] Santner, Thomas J and Williams, Brian J and Notz, William I and Williams, Brain J. *The design and analysis of computer experiments*, volume 1. Springer, 2003.

[16] Fedorov, Valerii V and Hackl, Peter. *Model-oriented design of experiments*, volume 125. Springer Science & Business Media, 2012.

[17] Nicholson, Ru. FEM4Marah. Finite Element Method Notes, 2020.

[18] Larson, Mats G and Bengzon, Fredrik. *The finite element method: theory, implementation, and applications*, volume 10. Springer Science & Business Media, 2013.

[19] Kelly, Piaras. Solid Mechanics. *Part II, Lecture notes, The University of Auckland*, 2020.

[20] Virtanen, Pauli and Gommers, Ralf and Oliphant, Travis E. and Haberland, Matt and Reddy, Tyler and Cournapeau, David and Burovski, Evgeni and Peterson, Pearu and Weckesser, Warren and Bright, Jonathan and van der Walt, Stéfan J. and Brett, Matthew and Wilson, Joshua and Millman, K. Jarrod and Mayorov, Nikolay and Nelson, Andrew R. J. and Jones, Eric and Kern, Robert and Larson, Eric and Carey, C J and Polat, İlhan and Feng, Yu and Moore, Eric W. and VanderPlas, Jake and Laxalde, Denis and Perktold, Josef and

Cimrman, Robert and Henriksen, Ian and Quintero, E. A. and Harris, Charles R. and Archibald, Anne M. and Ribeiro, Antônio H. and Pedregosa, Fabian and van Mulbregt, Paul and SciPy 1.0 Contributors. SciPy 1.0: Fundamental Algorithms for Scientific Computing in Python. *Nature Methods*, 17:261–272, 2020.

[21] Pawitan, Yudi. *In all likelihood : statistical modelling and inference using likelihood*. 2001.

[22] Simpson, Matthew J and Baker, Ruth E and Vittadello, Sean T and Maclaren, Oliver J. Practical parameter identifiability for spatio-temporal models of cell invasion. *Journal of the Royal Society Interface*, 17(164):20200055, 2020.

[23] Shahin, Marah. Optimal Experimental Design for Understanding Burn Injuries - Evidence Portfolio. Technical report, The University of Auckland, August 2020.

[24] Engineering ToolBox. Water - Thermal Diffusivity.

[25] Christine J. Andrews, Leila Cuttle, and Matthew J. Simpson. Quantifying the role of burn temperature, burn duration and skin thickness in an in vivo animal skin model of heat conduction. *International Journal of Heat and Mass Transfer*, 101:542–549, October 2016.

Appendices

A Finite Difference Stencil Derivation

The finite difference method approximates the equation of interest. In this project, the heat equation below is approximated.

$$\frac{\partial u}{\partial t} = \frac{\partial}{\partial x}\left(D\frac{\partial u}{\partial x}\right)$$

The explicit finite difference stencil used in this project is derived from the Taylor series.

$$\begin{aligned} f(x) &= \sum_{k=0}^{\infty} \frac{f^{(k)}(x_0)}{k!}(x-x_0)^k \\ &= f(x_0) + f'(x_0)(x-x_0) + \frac{f''(x_0)}{2!}(x-x_0)^2 + \frac{f'''(x_0)}{3!}(x-x_0)^3 + ... \end{aligned}$$

The terms $\frac{\partial u}{\partial t}$ and $\frac{\partial^2 u}{\partial x^2}$ were substituted by individual Taylor series approximations: two point forward and three point central equations for $\frac{\partial u}{\partial t}$ and $\frac{\partial^2 u}{\partial x^2}$, respectively. These equations together form the four point explicit stencil implemented in this project.
Therefore, to apply the series to $u(t)$ and $u(x)$ the Taylor series expansion was adapted.

First, $u(t)$. So, the Taylor series expansion of $u(t^{n+1})$ about t^n:

$$u(t^{n+1}) = u(t^n) + \Delta t\frac{du(t^n)}{dt} + \frac{(\Delta t)^2}{2}\frac{d^2u(t^n)}{dt^2} + \frac{(\Delta t)^3}{3!}\frac{d^3u(t^n)}{dt^3} + ...$$

The series was then truncated at $k = 2$ and rearranged for $\frac{du}{dt}$ (as needed for the heat equation):

$$\frac{du(t^n)}{dt} \approx \underbrace{\frac{u(t^{n+1}) - u(t^n)}{\Delta t}}_{\text{finite difference}} - \underbrace{\frac{\Delta t}{2}\frac{d^2u(t^n)}{dt^2}}_{\text{truncation error}}$$

Where the first term is the two point forward finite difference equation and the second term represents the truncation error.

Next $u(x)$. To create the three point central equation, both approximations about

$u(x_{i+1})$ and $u(x_{i-1})$ need to be considered.

$$u(x_{i+1}) = u(x_i) + \Delta x \frac{du(x_i)}{dx} + \frac{(\Delta x)^2}{2}\frac{d^2u(x_i)}{dx^2} + \frac{(\Delta x)^3}{3!}\frac{d^3u(x_i)}{dx^3} + \frac{(\Delta x)^4}{4!}\frac{d^4u(x_i)}{dx^4} + ...$$

$$u(x_{i-1}) = u(x_i) - \Delta x \frac{du(x_i)}{dx} + \frac{(\Delta x)^2}{2}\frac{d^2u(x_i)}{dx^2} - \frac{(\Delta x)^3}{3!}\frac{d^3u(x_i)}{dx^3} + \frac{(\Delta x)^4}{4!}\frac{d^4u(x_i)}{dx^4} + (-1)^k ...$$

Here, the approximations were truncated at $k = 4$ to ensure the truncation error is considered. Hence, $u(x_{i+1})$ and $u(x_{i-1})$ are added to give:

$$u(x_{i+1}) + u(x_{i-1}) = 2u(x_i) + 2\frac{(\Delta x)^2}{2}\frac{d^2u(x_i)}{dx^2} + 2\frac{(\Delta x)^4}{4!}\frac{d^4u(x_i)}{dx^4}$$

This equation above was then rearranged for $\frac{d^2u(x_i)}{dx^2}$ as per the heat equation.

$$\frac{d^2u(x_i)}{dx^2} \approx \underbrace{\frac{u(x_{i+1}) - 2u(x_i) + u(x_{i-1})}{(\Delta x)^2}}_{\text{finite difference}} - \underbrace{\frac{(\Delta x)^2}{12}\frac{d^4u(x_i)}{dx^4}}_{\text{truncation error}}$$

Therefore, plugging these finite difference equations back into the heat equation results in the following approximation (truncation errors above have not been included but considered):

$$\frac{u(t^{n+1}) - u(t^n)}{\Delta t} = D\frac{u(x_{i+1}) - 2u(x_i) + u(x_{i-1})}{(\Delta x)^2}$$

Given initial and boundary conditions are specified, the only unknown in this equation is $u(t^{n+1})$. The equation rearranged for this unknown gives:

$$u(x_i, t^{n+1}) = ru(x_{i+1}, t^n) + (1 - 2r)u(x_i, t^n) + ru(x_{i-1}, t^n)$$

$$\text{With,} \quad r = \frac{D\Delta t}{(\Delta x)^2}$$

The stencil was then applied iteratively to the mesh to numerically solve the equation at the points specified.

B Diffusivity Function: Representing Multiple Layers

```
#define thermal diffusivity
def D(x):
    if x<interface1:
        return D1*1e-06
    elif x<interface2:
        return D2*1e-06
    else:
        return D3*1e-06
```

C Synthetic Data: Linear Uncertainty Results

	Lower Bound	$D_{1,rec}$	Upper Bound	Widths
One Layer, One Probe	9.11E-08	9.12E-08	9.14E-08	3.54E-10
One Layer, Two Probes	9.06E-08	9.08E-08	9.10E-08	3.54E-10
One Layer, Three Probes	8.97E-08	8.98E-08	8.99E-08	2.04E-10
One Layer, All Points	9.09E-08	9.09E-08	9.09E-08	1.01E-12
Two Layer, Two Probes	9.15E-08	9.15E-08	9.16E-08	7.50E-11
Two Layer, All Points	9.09E-08	9.09E-08	9.09E-08	3.03E-13
Three Layer, Three Probes	9.08E-08	9.09E-08	9.09E-08	6.23E-11
Three Layer, All Points	9.09E-08	9.09E-08	9.09E-08	3.71E-13
Inputted D_1	-	9.09E-08	-	-

Table 6: D_1 95% confidence intervals for synthetic data

	Lower Bound	$D_{2,rec}$	Upper Bound	Widths
Two Layer, Two Probes	2.08E-06	3.06E-06	4.05E-06	1.97E-06
Two Layer, All Points	6.74E-07	6.76E-07	6.77E-07	2.75E-09
Three Layer, Three Probes	8.74E-09	2.75E-07	4.63E-07	3.76E-07
Three Layer, All Points	8.08E-07	8.10E-07	8.11E-07	2.54E-09
Inputted D_2	-	7.68E-07	-	-

Table 7: D_2 95% confidence intervals for synthetic data

	Lower Bound	$D_{3,rec}$	Upper Bound	Widths
Three Layer, Three Probes	-1.53E-05	1.93E-07	1.57E-05	3.10E-05
Three Layer, All Points	1.47E-09	1.69E-09	1.91E-09	4.37E-10
Inputted D_3	-	6.00E-06	-	-

Table 8: D_3 95% confidence intervals for synthetic data

D Additional Experimental Results

Experiment	Lower Bound	D_{rec}	Upper Bound	Widths
One Probe Exp 1	1.47E-01	1.49E-01	1.52E-01	4.74E-03
One Probe Exp 2	2.29E-01	2.29E-01	2.30E-01	1.22E-03
One Probe Exp 3	8.92E-02	9.21E-02	9.49E-02	5.69E-03
One Probe Exp 4	8.38E-02	8.61E-02	8.85E-02	4.76E-03
One Probe Exp 5	9.77E-02	9.91E-02	1.00E-01	2.76E-03
(M) One Probe Exp 1	1.62E-01	1.63E-01	1.64E-01	2.48E-03
(M) One Probe Exp 2	1.33E-01	1.35E-01	1.36E-01	3.30E-03
(M) One Probe Exp 3	2.73E-01	2.74E-01	2.75E-01	1.90E-03
(M) One Probe Exp 4	1.42E-01	1.44E-01	1.45E-01	3.17E-03
Two Probe Exp 1	1.17E-01	1.17E-01	1.17E-01	3.05E-04
Two Probe Exp 2	6.35E-02	6.36E-02	6.37E-02	2.52E-04
Two Probe Exp 3	9.61E-02	9.62E-02	9.63E-02	2.16E-04
Two Probe Exp 4	9.60E-02	9.61E-02	9.63E-02	2.66E-04
(M) Two Probe Exp 1	2.14E-01	2.14E-01	2.14E-01	4.58E-04
(M) Two Probe Exp 2	2.27E-01	2.27E-01	2.27E-01	5.27E-04
(M) Two Probe Exp 3	2.32E-01	2.32E-01	2.33E-01	5.64E-04
(M) Two Probe Exp 4	2.09E-01	2.10E-01	2.10E-01	5.05E-04
(M) Three Probe Exp 1	2.01E-01	2.01E-01	2.02E-01	1.39E-04
(M) Three Probe Exp 2	1.74E-01	1.74E-01	1.74E-01	1.15E-04
(M) Three Probe Exp 3	2.00E-01	2.00E-01	2.00E-01	1.43E-04
(M) Three Probe Exp 4	2.16E-01	2.16E-01	2.16E-01	1.62E-04

Table 9: D_1 95% confidence intervals for all one layer experiments

All values are (E-06). Where M represents whether the experiment had a modified boundary probe (measuring temperature directly below the aluminium disc) or an unmodified boundary probe (measuring temperature in the middle of the aluminium

disc).

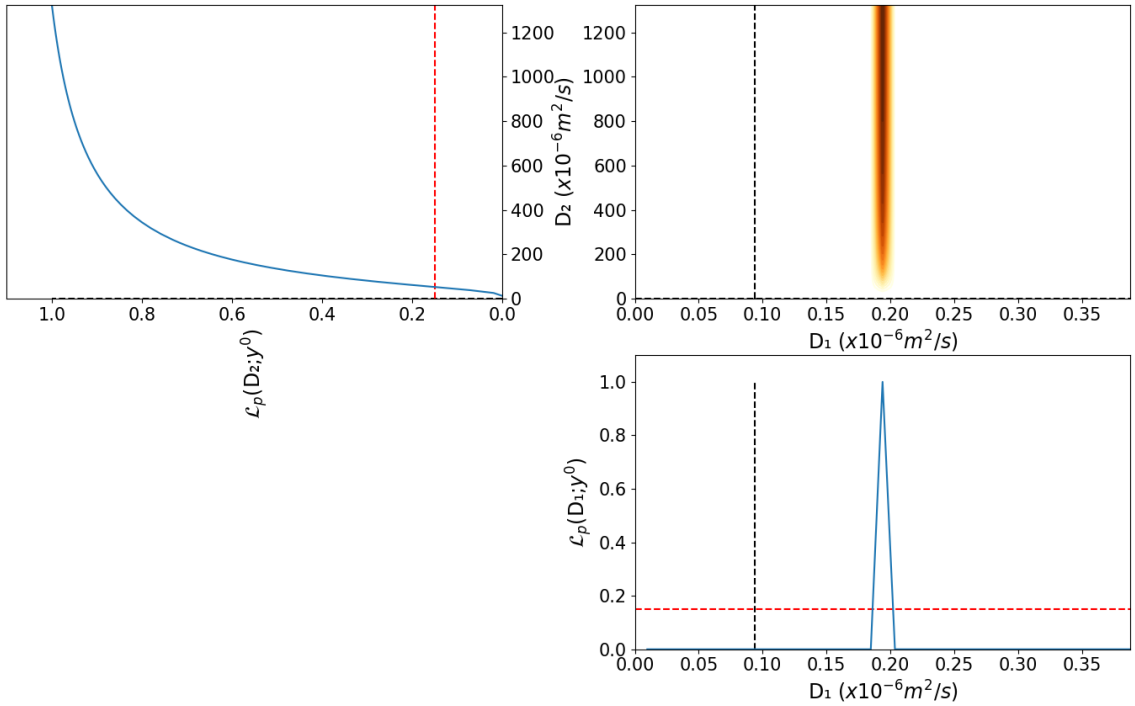

Figure 17: Two layer Experiment 4: likelihood profiles